The influence of diameter on the magnetic saturation in $Fe_{84}Cu_{16}$/MgO [001] multilayered islands

Tobias Warnatz[a,*], Björn Erik Skovdal[a], Fridrik Magnus[b], Henry Stopfel[a,1], Daniel Primetzhofer[a], Aaron Stein[c], Rimantas Brucas[d], Björgvin Hjörvarsson[a]

[a] *Department of Physics and Astronomy, Uppsala University, Box 516, SE-75120 Uppsala, Sweden*
[b] *Science Institute, University of Iceland, Dunhaga 3, IS-107 Reykjavik, Iceland*
[c] *Center for Functional Nanomaterials, Brookhaven National Laboratory, Upton, New York 11973, USA*
[d] *Department of Engineering Sciences, Uppsala University, Box 534, SE-75121 Uppsala, Sweden*

Abstract

The saturation field of circular islands, consisting of $[Fe_{84}Cu_{16}/MgO]_9Fe_{84}Cu_{16}$ multilayers, increases with decreasing diameter of the islands. When the diameter of the islands is below 450 nm the field induced changes are dominated by a coherent rotation of the moment of the $Fe_{84}Cu_{16}$ layers. For diameters of 2 μm and larger, a signature of domain nucleation and evolution is observed. The changes in the saturation field with diameter of the islands are ascribed to the interplay between interlayer exchange coupling, stray field coupling at the edges and the crystalline anisotropy of the $Fe_{84}Cu_{16}$ layers.

1. Introduction

The large magnetoresistance of Fe/MgO/Fe junctions makes them highly relevant within basic as well as applied sciences [1–3]. An interlayer exchange coupling (IEC) across the insulating MgO layers has been observed, which in turn influences the field induced switching of the magnetic layers [4]. The IEC between the Fe layers, in conjunction with their magnetocrystalline anisotropy can be utilized to influence the magnetic order, which can for example be used for obtaining sequential switching of the magnetization of the layers [5, 6]. The remanent states and switching behavior depend on the relative strength of the IEC and the anisotropy [7]. Furthermore, the IEC strongly depends on the crystalline quality , thickness and stoichiometry of the MgO layer [4–11] whereas the magnetic anisotropy can be influenced by alloying the magnetic layer. For example, alloying Fe with small amounts of Cu reduces the magnetocrystalline anisotropy [12] while retaining bcc structure [13]. When patterning multilayered structures into islands, an additional energy term needs to be considered: the magnetostatic energy arising from the stray field at the edges of the magnetic layers [14–16].

Here, we show that the magnetic switching in multilayered circular islands depends strongly on the diameter of the islands, reflecting the relative importance of the interlayer exchange coupling and magnetic anisotropy versus the stray field coupling at the edges of the islands. These findings are important for example for the miniaturization of multiple back-to-back magnetic tunnel junctions.

2. Experimental Methods

The $Fe_{84}Cu_{16}$/MgO multilayers were grown by magnetron sputtering. The base pressure of the chamber was below 2×10^{-9} mbar and the operating pressure of the Ar sputtering gas (99.999 99%) was 2.7×10^{-3} mbar. The MgO(001) substrates ($10 \times 10 \times 1$ mm^3) were annealed for 1h at 550 °C. The substrate temperature was thereafter lowered and kept constant at 165 °C during the sample growth. The $Fe_{84}Cu_{16}$ layers (2.0 nm thick) were deposited by dc sputtering while the oxide layers (1.7 nm thick) were prepared by rf sputtering from a MgO target. After growing 9

*Corresponding author
Email address: Tobias.Warnatz@physics.uu.se (Tobias Warnatz)
[1] Present Address: Department of Engineering Sciences, Uppsala University, Box 534, SE-75121 Uppsala, Sweden

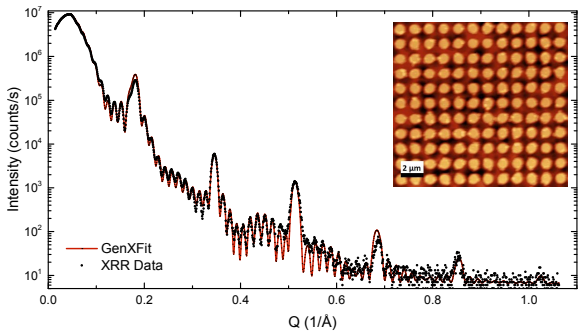

Figure 1: XRR measurement and fit obtained from an unpatterned $Fe_{84}Cu_{16}$/MgO [001] multilayer. The inset is an atomic force microscopy image of the 450 nm islands.

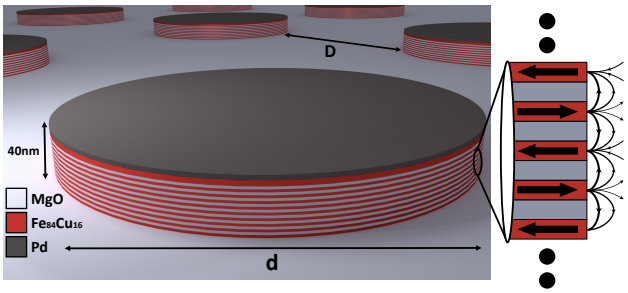

Figure 2: Schematic illustration of the patterned structures. The red discs represent $Fe_{84}Cu_{16}$, the oxide layers and the MgO substrate are light grey. The dark grey discs represent Pd capping layers. The right hand picture illustrates the magnetic alignment (black arrows) of individual $Fe_{84}Cu_{16}$ layers and their exhibited stray field.

$Fe_{84}Cu_{16}$/MgO bilayers, a thick (3.5 nm) $Fe_{84}Cu_{16}$ layer was deposited and capped at room temperature with a Pd layer (4.8 nm thick). The Pd capping layer prevents the oxidation of the underlying sample and increases the magnetic moment of the outermost layer. A $[Fe(2.2nm)/MgO(1.7nm)]_{10}Pd$ reference sample was grown under the same conditions as described above.

The composition of the samples was determined using Rutherford Backscattering Spectrometry (RBS) at the Tandem laboratory in Uppsala, while the structural quality was determined by X-ray analysis using a Philips X-Pert Pro MRD diffractometer (Cu K_α = 1.5418 Å). X-ray reflectivity (XRR) measurements were used to determine the thickness of the layers and their interface roughness (fitted with GenX [17]) as illustrated in figure 1. The GenX fit yields top-interface root mean square roughnesses of 3.3 Å ($Fe_{84}Cu_{16}$) and 2.3 Å (MgO) and confirms the intended layer thicknesses. The RBS-measurements confirmed the Fe:Cu ratio of 84:16 but revealed a Mg:O ratio of 1:4, which can be attributed to an oxidation of the magnetic layers at the interfaces. The X-ray diffraction (XRD) measurement (not shown) demonstrated limited coherency between the layers, in a similar way as described in Ref. 18. The presence of Cu in the Fe layers decreases the overall structural coherency of the samples while the layering can be viewed as retained.

Extended arrays of circular islands (150 nm, 300 nm, 450 nm, 2 μm and 4 μm in diameter) were patterned. A schematic illustration of the resulting structure is provided in figure 2. The inter-island distance D was either equal to (sub-micrometer islands) or half of (micro-meter islands) the island diameter d to prevent magnetic interactions between adjacent islands (as reproduced by micromagnetic simulations). Hence, magnetization measurements representative of a single island can be performed on the patterned arrays. The islands in the submicrometer region were patterned by a combination of electron-beam lithography and argon-milling at the Center for Functional Nanomaterials, which is part of the Brookhaven National Laboratory. The larger islands (2 and 4 μm in diameter) were patterned at the Microstructure Laboratory in Uppsala, using optical lithography. Atomic force microscopy measurements (contact mode) were performed on the patterned samples to verify the diameter and spacing of the islands, as *e.g.* illustrated in the inset in figure 1. The imaging shows that the pattern is well defined and reasonably free of defects over extended areas.

3. Results and Discussion

Magnetization measurements were carried out at room temperature before and after patterning, using a magneto-optical-Kerr-effect setup in longitudinal geometry with *s*-polarized light. The magnetic field was applied in the plane of the sample and the magnetic response was measured parallel to the applied field. Representative hysteresis loops of continuous thin films and a patterned array are displayed in figure 3. A four-fold magnetocrystalline anisotropy is revealed in the multilayers, in addition to a hysteresis with discrete steps (often referred to as digital hysteresis) along the magnetic easy axis (the $Fe_{84}Cu_{16}$ [100] axis). This is a result of an antiferromagnetic interlayer exchange coupling between

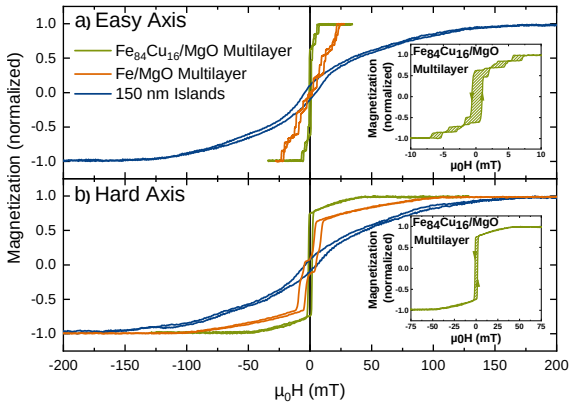

Figure 3: Room-temperature, in-plane magnetization measurements along the easy (a) and hard (b) axes of unpatterned $Fe_{84}Cu_{16}$/MgO (green line) and Fe/MgO (orange line) multilayers as well as patterned $Fe_{84}Cu_{16}$/MgO islands with a diameter of 150 nm (blue line). The insets are a zoom in of the hysteresis loops of the unpatterned $Fe_{84}Cu_{16}$/MgO multilayer.

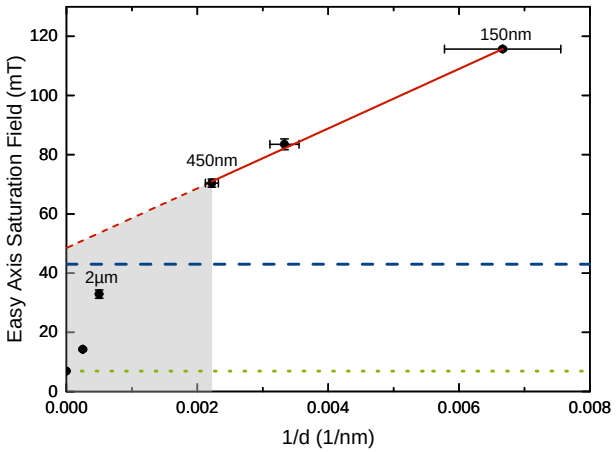

Figure 4: The saturation field (95% threshold) of $Fe_{84}Cu_{16}$/MgO multilayers, as a function of the inverse diameter ($1/d$). The solid red line is a linear fit of the data. The dotted, green line represents the saturation field of the thin film easy axis and the dashed, blue line corresponds to the saturation field of the thin film in-plane hard axis. The grey area marks the region, which cannot be described without invoking domain formation and propagation.

the $Fe_{84}Cu_{16}$ layers through the MgO. A measurement along the magnetic in-plane hard axis (the $Fe_{84}Cu_{16}$ [110] axis) is illustrated in the inset of figure 3b. The strength of the interlayer exchange coupling can be determined from the saturation field in the easy axis direction (7 mT), whereas the strength of the magnetocrystalline anisotropy can be determined from the saturation field of the in-plane hard axis (∼43 mT). The relatively strong four-fold magnetocrystalline anisotropy compared to the antiferromagnetic interlayer exchange coupling can result in a 90° remanent configuration of the adjacent magnetic $Fe_{84}Cu_{16}$ layers upon field cycling. This configuration is apparent from the remanent magnetization value ($\sim 0.5 M_s$) which has previously been demonstrated [5, 7].

A significantly higher saturation field (along the magnetic easy axis) is obtained for Fe/MgO superlattices, as compared to $Fe_{84}Cu_{16}$/MgO multilayers. As illustrated in figure 3a, a saturation field of 23 mT as compared to 7 mT, is obtained for Fe and $Fe_{84}Cu_{16}$ layers. The larger interlayer exchange coupling in pure Fe layers gives rise to antiferromagnetic ordering and consequently zero remanence [6]. Furthermore, the saturation field along the in-plane hard axis is increased to ∼100 mT (fig. 3b) which is consistent with a stronger magnetocrystalline anisotropy in the Fe, as compared to the FeCu alloy under similar strain conditions (biaxial tensile strain). Thus, alloying with Cu results in a reduction of the anisotropy and the interlayer exchange coupling.

Patterning the $Fe_{84}Cu_{16}$/MgO multilayers into circular islands has a pronounced effect on the observed magnetic properties, as seen in figure 3. The steps in the easy axis hysteresis loop disappear, the remanence is reduced and the saturation field is seen to increase. For islands with diameters about 450 nm and smaller, the magnetic response is close to isotropic as expected from structures dominated by stray field coupling at the edges of the islands, see figure 2.

The influence of the stray field coupling can easily be calculated when the rotation of the moment is assumed to be single domain and collinear: The stray field coupling between the magnetic layers is proportional to the magnetization multiplied by the outer surface area of the $Fe_{84}Cu_{16}$ layers. By the same token, the coupling of the magnetic layers to the external field scales with the volume multiplied by the magnetization of the magnetic layers. In the absence of anisotropy and interlayer exchange coupling the saturation field of multilayered islands can therefore be expressed as:

$$H_{\mathrm{sat}} \propto \frac{A_{\mathrm{os}}}{V_{\mathrm{d}}} = \frac{\pi \cdot t \cdot d}{1/4\pi \cdot t \cdot d^2} \propto \frac{1}{d} \qquad (1)$$

with the $Fe_{84}Cu_{16}$ outer surface area A_{os}, disk volume V_{d}, thickness t and diameter d. This relation

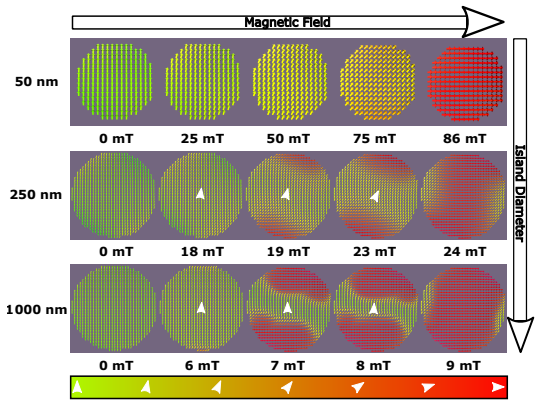

Figure 5: Simulations of the field dependence of Fe-alloy/Vacuum/Fe-alloy trilayers with various island diameters using $MuMax^3$. For clarity, only one of the layers is displayed.

can be generalized to:

$$H_{\mathrm{sat}} = H_{\mathrm{x}} + \frac{C}{d} \tag{2}$$

where we have included a material dependent saturation field for an infinite extension (H_{x}), still assuming coherent rotation of the magnetization. H_{x} consists of contributions from the anisotropy as well as the exchange coupling while C is inversely proportional to the distance between adjacent magnetic layers (here C is a constant). Hence, the overall impact of the stray field coupling becomes larger with decreasing island size, as discussed in references [14–16]. Consequently, a linear increase of the saturation field with the inverse island diameter is expected, as long as the layers are single domain and rotate coherently.

As seen in figure 4, the saturation field is found to scale with the inverse island diameter when d is equal to or less than 450 nm. When the diameter is larger, the single domain picture is not expected to hold, resulting in a gradual transition towards a nucleation switching of the layers. The saturation field of a coherently rotating, single domain thin film (infinite d) is governed by the film's magnetocrystalline anisotropy (∼43 mT, see fig. 3 b.). This value corresponds well to the extrapolated value from our model, which is determined to be $H_{\mathrm{x}} \sim 49$ mT (intercept with the y-axis).

To explore the validity of the interpretation of the observed changes we performed micromagnetic simulations of circular Fe-alloy/Vacuum/Fe-alloy trilayers with diameters $d = 50 - 1000$ nm. The composition of the sample is not of major concern as we are exploring the possibility of a transition from a collinear to non-collinear response of multilayered islands. We used the GPU-accelerated micromagnetic simulation program $MuMax^3$ [19] for these calculations. The 2.0 nm thick Fe-alloy layers were separated by 1.7 nm and a saturation magnetization $M_{\mathrm{s}} = 1.76 \times 10^6$ A/m (bulk iron), an exchange stiffness constant $A_{\mathrm{ex}} = 21$ pJ/m and a cubic anisotropy constant $K_{\mathrm{c}} = 4.7 \times 10^4$ J/m^3 (bulk iron) were used. No temperature effects were considered. The magnetocrystalline anisotropy of the biaxially strained Fe and $Fe_{84}Cu_{16}$ layers is larger as compared to their unstrained state. However, the presence of Cu reduces the magnetocrystalline anisotropy of the alloy as compared to pure Fe (see fig. 3), resulting in an anisotropy field which is close to identical to unstrained Fe [20]. Therefore, the anisotropy constant of bulk Fe can be used to model this system reasonably well. Fully coherent rotation is observed for islands with $d < 150$ nm (50 nm in fig. 5). Above this point, the rotation begins to appear non-collinear, forming textures (as seen in the results for 250 nm islands in fig. 5). With further increase in diameter, the textured rotation gradually becomes more prominent until clear domain switching is observed (see 1000 nm islands in fig. 5). The simulations thereby confirm the basis of our assumptions and provide a qualitative description of the textures involved, as illustrated in figure 5.

4. Conclusion

To conclude, we have shown that the magnetic response of multilayered islands can be tuned by changing the composition of the magnetic layer as well as changing the diameter of the patterned islands. Alloying Fe with Cu reduces the magnetocrystalline anisotropy, but also the interlayer exchange coupling. Reducing the diameter of multilayered islands leads to an increased saturation field. By tuning the stray field coupling (by altering the island diameter) [16], magnetocrystalline anisotropy (*e.g.* by alloying with Cu) [12] and interlayer exchange coupling (by altering the thickness of the insulating layer) [4, 5] the magnetic response can be tailored almost at will.

Acknowledgments

This work was funded by the Swedish research council (VR) and the Knut and Alice Wallenberg foundation (KAW). The electron-beam lithography patterning was performed at the Center for Functional Nanomaterials, Brookhaven National Laboratory, which is supported by the U.S. Department of Energy, Office of Basic Energy Sciences, under Contract No. DE-SC0012704. FM acknowledges funding from the Icelandic Centre for Research, grant no. 174271-051. Support by VR-RFI (contract # 821-2012-5144) and the Swedish Foundation for Strategic Research (SSF, contract RIF14-0053) supporting accelerator operation is gratefully acknowledged. The authors are grateful to Ioan-Augustin Chioar for support with electron-beam lithography. The authors thank Vassilios Kapaklis and Gunnar Karl Pálsson for stimulating discussions. The authors acknowledge Agne Ciuciulkaite for support with micromagnetic simulations.

References

[1] S. Yuasa, T. Nagahama, A. Fukushima, Y. Suzuki, K. Ando, Giant room-temperature magnetoresistance in single-crystal Fe/MgO/Fe magnetic tunnel junctions, Nature Materials 3 (2004) 868–871. URL: http://www.nature.com/doifinder/10.1038/nmat1257. doi:10.1038/nmat1257.

[2] S. S. P. Parkin, C. Kaiser, A. Panchula, P. M. Rice, B. Hughes, M. Samant, S.-H. Yang, Giant tunnelling magnetoresistance at room temperature with MgO (100) tunnel barriers, Nature Materials 3 (2004) 862–867. URL: http://www.nature.com/doifinder/10.1038/nmat1256. doi:10.1038/nmat1256.

[3] C. Chappert, A. Fert, F. N. Van Dau, The emergence of spin electronics in data storage, Nature Materials 6 (2007) 813. URL: http://dx.doi.org/10.1038/nmat2024.

[4] J. Faure-Vincent, C. Tiusan, C. Bellouard, E. Popova, M. Hehn, F. Montaigne, A. Schuhl, Interlayer Magnetic Coupling Interactions of Two Ferromagnetic Layers by Spin Polarized Tunneling, Physical Review Letters 89 (2002). URL: http://link.aps.org/doi/10.1103/PhysRevLett.89.107206. doi:10.1103/PhysRevLett.89.107206.

[5] R. Moubah, F. Magnus, T. Warnatz, G. K. Palsson, V. Kapaklis, V. Ukleev, A. Devishvili, J. Palisaitis, P. O. å. Persson, B. Hjörvarsson, Discrete Layer-by-Layer Magnetic Switching in Fe / MgO (001) Superlattices, Physical Review Applied 5 (2016). URL: http://link.aps.org/doi/10.1103/PhysRevApplied.5.044011. doi:10.1103/PhysRevApplied.5.044011.

[6] F. Magnus, T. Warnatz, G. K. Palsson, A. Devishvili, V. Ukleev, J. Palisaitis, P. O. å. Persson, B. Hjörvarsson, Sequential magnetic switching in Fe/MgO(001) superlattices, Physical Review B 97 (2018). URL: https://link.aps.org/doi/10.1103/PhysRevB.97.174424. doi:10.1103/PhysRevB.97.174424.

[7] C. Bellouard, J. Faure-Vincent, C. Tiusan, F. Montaigne, M. Hehn, V. Leiner, H. Fritzsche, M. Gierlings, Interlayer magnetic coupling in Fe/MgO junctions characterized by vector magnetization measurements combined with polarized neutron reflectometry, Physical Review B 78 (2008). URL: http://link.aps.org/doi/10.1103/PhysRevB.78.134429. doi:10.1103/PhysRevB.78.134429.

[8] M. Y. Zhuravlev, E. Y. Tsymbal, A. V. Vedyayev, Impurity-Assisted Interlayer Exchange Coupling across a Tunnel Barrier, Physical Review Letters 94 (2005). URL: http://link.aps.org/doi/10.1103/PhysRevLett.94.026806. doi:10.1103/PhysRevLett.94.026806.

[9] T. Katayama, S. Yuasa, J. Velev, M. Y. Zhuravlev, S. S. Jaswal, E. Y. Tsymbal, Interlayer exchange coupling in Fe/MgO/Fe magnetic tunnel junctions, Applied Physics Letters 89 (2006) 112503. URL: http://aip.scitation.org/doi/10.1063/1.2349321. doi:10.1063/1.2349321.

[10] A. Kozioł-Rachwał, T. Ślęzak, M. Ślęzak, K. Matlak, E. Młyńczak, N. Spiridis, J. Korecki, Antiferromagnetic interlayer exchange coupling in epitaxial Fe/MgO/Fe trilayers with MgO barriers as thin as single monolayers, Journal of Applied Physics 115 (2014) 104301. URL: http://scitation.aip.org/content/aip/journal/jap/115/10/10.1063/1.4867745. doi:10.1063/1.4867745.

[11] H. X. Yang, M. Chshiev, A. Kalitsov, A. Schuhl, W. H. Butler, Effect of structural relaxation and oxidation conditions on interlayer exchange coupling in Fe|MgO|Fe tunnel junctions, Applied Physics Letters 96 (2010) 262509. URL: http://scitation.aip.org/content/aip/journal/apl/96/26/10.1063/1.3459148. doi:10.1063/1.3459148.

[12] Z. Tian, C. S. Tian, L. F. Yin, D. Wu, G. S. Dong, X. Jin, Z. Q. Qiu, Magnetic ordering and anisotropy of epitaxially grown Fe x Cu 1 - x alloy on GaAs (001), Physical Review B 70 (2004). URL: https://link.aps.org/doi/10.1103/PhysRevB.70.012301. doi:10.1103/PhysRevB.70.012301.

[13] C. L. Chien, S. Liou, D. Kofalt, W. Yu, T. Egami, T. J. Watson, T. R. McGuire, Magnetic properties of Fe x Cu 100- x solid solutions, Physical Review B 33 (1986) 3247. URL: https://journals.aps.org/prb/abstract/10.1103/PhysRevB.33.3247.

[14] M. v. Kampen, I. L. Soroka, R. Bručas, B. Hjörvarsson, R. Wieser, K. D. Usadel, M. Hanson, O. Kazakova, J. Grabis, H. Zabel, C. Jozsa, B. Koopmans, On the realization of artificial XY spin chains, Journal of Physics: Condensed Matter 17 (2005) L27–L33. URL: http://stacks.iop.org/0953-8984/17/i=2/a=L04?key=crossref.59b9dc902ec2de4fe968b6a10ab757d5. doi:10.1088/0953-8984/17/2/L04.

[15] A. A. Fraerman, B. A. Gribkov, S. A. Gusev, A. Y. Klimov, V. L. Mironov, D. S. Nikitushkin, V. V. Rogov, S. N. Vdovichev, B. Hjorvarsson, H. Zabel, Magnetic force microscopy of helical states in multilayer nanomagnets, Journal of Applied Physics 103 (2008) 073916. URL: http://aip.scitation.org/doi/10.1063/1.2903136. doi:10.1063/1.2903136.

[16] A. Kozioł-Rachwał, W. Skowroński, M. Frankowski,

J. Chęciński, S. Ziętek, P. Rzeszut, M. Ślęzak, K. Matlak, T. Ślęzak, T. Stobiecki, J. Korecki, Interlayer exchange coupling, dipolar coupling and magnetoresistance in Fe/MgO/Fe trilayers with a subnanometer MgO barrier, Journal of Magnetism and Magnetic Materials 424 (2017) 189–193. URL: http://linkinghub.elsevier.com/retrieve/pii/S030488531631664X. doi:10.1016/j.jmmm.2016.09.131.

[17] M. Björck, G. Andersson, *GenX* : an extensible X-ray reflectivity refinement program utilizing differential evolution, Journal of Applied Crystallography 40 (2007) 1174–1178. URL: http://scripts.iucr.org/cgi-bin/paper?S0021889807045086. doi:10.1107/S0021889807045086.

[18] H. Raanaei, H. Lidbaum, A. Liebig, K. Leifer, B. Hjörvarsson, Structural coherence and layer perfection in Fe/MgO multilayers, Journal of Physics: Condensed Matter 20 (2008) 055212. URL: http://stacks.iop.org/0953-8984/20/i=5/a=055212?key=crossref.17566e27ae39a6136ff82fb301e05d81. doi:10.1088/0953-8984/20/5/055212.

[19] A. Vansteenkiste, J. Leliaert, M. Dvornik, M. Helsen, F. Garcia-Sanchez, B. Van Waeyenberge, The design and verification of MuMax3, AIP Advances 4 (2014) 107133. URL: http://aip.scitation.org/doi/10.1063/1.4899186. doi:10.1063/1.4899186.

[20] C. Kittel, Physical Theory of Ferromagnetic Domains, Reviews of Modern Physics 21 (1949) 547. URL: https://link.aps.org/doi/10.1103/RevModPhys.21.541. doi:10.1103/RevModPhys.21.541.